A turbines-module adapted to the marine site for tidal farms layout optimization

Micol Pucci, Debora Bellafiore, Stefania Zanforlin, and Antonio Frangioni

***Abstract*—We propose an improvement of existing methodologies for tidal farm layout optimization. We start with a standard discrete approach using a Mixed Integer Quadratic Programming (MIQP) formulation coupled with a wake model. Since the approach is discrete in nature one needs to establish a priori the available turbine locations in a staggered configuration. The novelty lies in the definition of the staggered configuration adopted as input of the optimization process, whereby the grid is tailor made for a particular ocean site of interest using geometrical and site dependent arguments. In particular, considering the range of prevalent flow directions characteristics of the site we establish the best "module" made up of three turbines, which is then used as the building block of the staggered grid. This allows us to adapt the approach to different sites while retaining its positive characteristics (ease of implementation and relative computational efficiency). The application of this methodology to a case study farm made up of 9 machines shows an increase in power production of about 6% compared to the configuration obtained by optimizing with a conventional staggered grid, and a nearly 10-times improvement of the power density.**

***Index Terms*—optimization, HATT, farm layout, MIQP, SHYFEM, BEM**

I. Introduction

In recent years, the need for increasing renewable energy generation is becoming more and more acute due to climate changes and geopolitical factors. In this framework, ocean energy plays an important role in clean energy production. Indeed, many companies worldwide are working on the development of tidal energy converters, reaching a Technology Readiness Level (TRL) of up to 7, and in some cases even commercial level (i.e., TRL 9) [1]. This is true in particular for Horizontal Axis Tidal Turbines (HATTs), which benefit of significant technological transfer from the know-how of the wind energy sector.

Since the sea and the ocean (floor) are matter of interest for different stakeholders, it is essential to plan and design tidal farms by maximising the power production of a given set of HATTs, so as to more quickly recoup the investment and running costs, while at the same time reducing the amount of occupied sea(floor). This justifies the large amount of scientific literature about farm layout optimization, especially in the wind field. The optimization process can be continuous or discrete: in the former the turbines' locations can be varied with continuity in the horizontal space, whereas in the latter turbines can only be placed in the available locations, which are established a-priori. The latter approach is simpler and computationally more efficient, and it is therefore usually preferred. One of its most common implementations is to build a Mixed Integer Quadratic Programming (MIQP) formulation of the problem using a wake model—the simplest and most popular one being that proposed by Jensen [2]—to describe the interaction of each pair of turbines. The MIQP model can then be solved by standard tools, possibly after having been linearised [3]–[5].

The discrete approach, however, requires a way to choose the available locations. How this is done is often not clearly discussed. Some assumptions are commonly adopted, such as that it is necessary to leave 5 turbine diameters between devices in the flow direction to grant a minimum wake recovery [6], and that a minimum technical distance must be kept between machines [7]. But there still is a large number of possible configurations that satisfy these assumptions, and little discussion is usually provided on how to choose among them. In general, a staggered configuration is chosen where turbines in odd columns are off from those in even ones by a fixed amount related to their diameters, and their distance is the above-mentioned 5 diameters. However, this rigid assignment does not take into account the characteristics of the chosen marine site, and in particular the prevalent flow directions; arguably, a bespoke grid should be able to improve the outcome of the optimization process.

In this work we will show that implementing such a strategy does indeed deliver some advantages. We will compare two optimization processes: one performed using a conventional staggered grid as input of the optimization algorithm ($grid_1$ in the following), and the other performed using a site-adapted grid ($grid_2$ in the following). Our development is as follows: in section II the adopted methodology is described, in section III a case study is analysed, and some conclusions are provided in section IV.

II. Methodology

A. Structure of the optimization algorithm

In this work we adopt as optimization process a MIQP algorithm based on the Jensen's wake model

M. Pucci is with the Department of Energy, Systems, Territory and Constructions Engineering of the University of Pisa, 56122 Pisa, Italy (micol.pucci@phd.unipi.it).

D. Bellafiore is with the Institute of Marine Sciences-National Research Council (ISMAR-CNR), Castello 2737/F, 30122 Venice, Italy (debora.bellafiore@ve.ismar.cnr.it).

S. Zanforlin is with the Department of Energy, Systems, Territory and Constructions Engineering of the University of Pisa, 56122 Pisa, Italy (stefania.zanforlin@unipi.it).

A. Frangioni is with the Department of Informatics of the University of Pisa, 56122 Pisa, Italy (antonio.frangioni@unipi.it).

Digital Object Identifier:
https://doi.org/10.36688/ewtec-2023-416

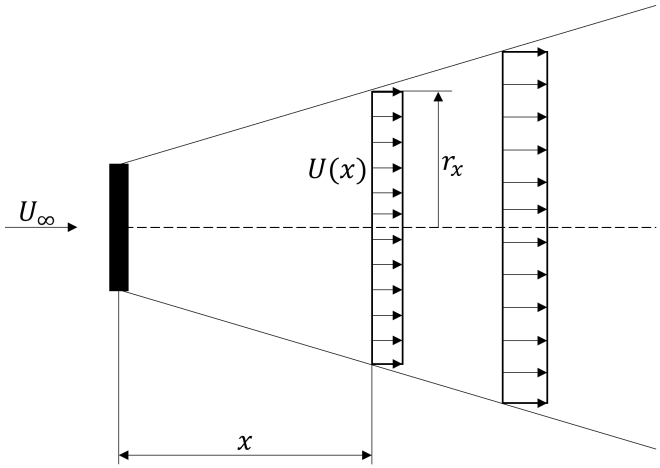

Fig. 1. Qualitative representation of the wake development in the Jensen's model.

for Horizontal Axis Turbines, which assumes a wake development described by

$$U(x) = U_\infty \cdot [1 - d] \tag{1}$$
$$d = 2a \cdot (r/r_x)^2 \tag{2}$$
$$r_x = \alpha x + r \tag{3}$$

where U_∞ is the undisturbed flow velocity, $U(x)$ is the wake velocity at a distance x downstream the turbine (the black rectangle in Fig.1), a is the axial induction factor imposed equal to $1/3$, r is the turbine radius, and $\alpha = 0.035$ is the wake expansion (the reason for this choice of the value will be discussed in section II-B). This is the basic formulation of the model: some improvements consist for instance in a gaussian shape velocity profile in the wake, instead of a uniform profile, but this improvement will not be considered here. This wake model was originally developed for wind turbines representation, but it can be extended to the tidal environment by tuning some parameters, as discussed in [8].
In Eq. (2), d represents the velocity deficit in the wake of a single turbine, so if only that turbine is present, d is sufficient to calculate the velocity at a generic x location as in Eq. (1). What if the velocity at the generic x location, is due to the contribution of multiple turbines, i. e. multiple wakes overlapping at x? As suggested in [3], the total kinetic energy deficit is the sum of the kinetic energy deficits of the individual turbines affecting location x. Since, the kinetic energy is proportional to the square of the velocity, $U(x)$ becomes

$$U(x) = U_\infty \cdot [1 - \sqrt{\sum_{i=1}^{N_t} d_{ij}^2}] \tag{4}$$
$$d_{ij}^2 = (2a \cdot (r/r_{x(ij)})^2)^2 \tag{5}$$

where N_t is the number of turbine present, d_{ij}^2 is the square of the wake velocity deficit on turbine j due to turbines i as computed via (2), $x(ij)$ is the distance between turbine i and j in the flow direction. Turbine i is affecting turbine j with its wake if the following condition

$$y(ij) \leq \alpha \cdot x(ij) + r \tag{6}$$

holds, where $y(ij)$ is the turbines transversal distance. Let now N_t be the number of turbine to place, p the number of available (discrete) locations, and k a binary variable of dimension p, which will be equal to 1 if the p-th position is occupied by a turbine and 0 otherwise. Let A be the $p \times p$ of the velocity deficit factor, i.e., such that $a_{ij} = 0$ if turbine i does not affect turbine j with its wake, and otherwise

$$a_{ij} = d_{ij}^2 \tag{7}$$

This allows to construct the matrix A.
The objective of the optimization is to maximize the power extraction, i.e., to minimize the wake interaction, and in particular the velocity deficit of the incoming flow on each turbine. This means minimizing the root term in Eq. 4 for each j turbine. This result in minimizing

$$\sum_{j=1}^{N_t} \sum_{i=1}^{N_t} d_{ij}^2 \tag{8}$$

The optimization problem model then is

$$\min k^T \cdot A \cdot k \tag{9}$$
$$\textstyle\sum_{g=1}^{p} k(g) = N_t \tag{10}$$
$$k(g) \in \{0, 1\} \qquad g = 1, \ldots, p \tag{11}$$

This is a MIQP that, for reasonable sizes, can be efficiently solved using off-the-shelf software.

B. Model test for a real-size turbine

The layout of the farm, which will result as output of the optimization process, will be tested using the SHYFM code, an Open Source Shallow Water equations software [9]. The SHYFEM code was equipped with a HATT model based on the Blade Element Momentum (BEM) theory, and will be used to compare several farm layouts. Hence, we have to guaratee that the SHYFEM turbine model correctly reproduces the fluid dynamics field all around the turbine. We had already tested and validated the model against experimental data for a prototype of 1m diameter, as reported in [10], but we want to ensure that a real-size turbine is also well described by the model, in terms of performance and velocity field. Unfortunately, we have no available experimental data of a real size turbine. However we can compare the results from the SHYFEM model to high fidelity CFD results. Hence, we consider as benchmark the real-size turbine proposed in [11], [12], which is geometrically similar to the one used in [10] for the prototype test. This turbine has a diameter $D_p = 10$m, and the computational domain in [11], [12] is a rectangular parallelepiped $5D_p$ wide, $5D_p$ deep, and $40D_p$ long, with the turbine located $10D_p$ downstream from the inlet. The undisturbed flow velocity is 3.1 m/s. For our simulation we adopted the same aforementioned set up. Moreover, the grid resolution in the turbine zone is $1/20$ of D_p.

We first analyse the performance of the device, in terms of power coefficient C_P at different Tip Speed Ratios TSRs, defined as

$$C_P = \frac{P}{1/2\rho A U_\infty^3} \tag{12}$$

$$TSR = \frac{r\Omega}{U_\infty} \tag{13}$$

where P is the produced power, ρ is the water density, A is the area swept by rotor's blades, and Ω is the rotational speed.

Fig. 2 depicts the high fidelity CFD results from [12], where it is shown that for high Reynolds numbers (order of magnitude 10^6), obtained by varying the turbine diameter or the undisturbed flow velocity, the performance curve is the single one shown. SHYFEM results (in red) show a small underestimate of the maximum C_P, but also of the optimal TSR (3 instead of 3.64).

Concerning the velocity field, and in particular the wake development, we compare our model with wake velocity profile of [11] from $1D_p$ to $15D_p$ downstream the turbine. The wake development in high fidelity CFD simulations is guaranteed by the fact that 160 turbine rotations were performed. In Fig. 3 we can observe a good agreement between the two simulated turbines in the near wake and until $3D_p$ downstream, while for the rest of the wake extension the SHYFEM model shows a faster recovery. The high fidelity CFD model, used as benchmark, assumes a 10% of turbulence intensity. However in CFD simulations, the inlet turbulence is not maintained throughout the domain (unless turbulence source terms are present). The more we move away from the inlet, the more the turbulence intensity is reduced. This aspect affects the wake development, so that in the far wake, even the high fidelity CFD cannot be considered representative of a case with high background turbulence (as in most tidal sites). Therefore, due to the limitations of both models, the behaviour of the SHYFEM turbine model can be considered satisfying, given the simplicity and the low computational time required for simulations (18 hours instead of 28 days of the high fidelity CFD).

We also wanted to check if Jensen's wake model, which was developed for wind applications, correctly predicts the behaviour of a tidal turbine, as already done in the literature [13], [8]. The alpha value suggested by Jensen for a typical wind wake is approximately 0.1. This value gives poor results in terms of wake centreline velocity and wake thickness compared to the SHYFEM tidal turbine model (but also compared to the high fidelity CFD). We have therefore tried to tune the variable to very low values: we found confirmation of an analogue approach in [8]. The latter reference shows that Jensen's model predictions fits well with CFD results by adopting a wake expansion coefficient $\alpha = 0.04$. Fig. 3 shows both the wake thickness and the wake velocity predicted by the Jensen's model at different alpha values. In Fig.4 we can also see the wake centreline velocity of the SHYFEM model compared to Jensen's model at several alpha values. We choose to set $\alpha = 0.035$, since it yields a good match

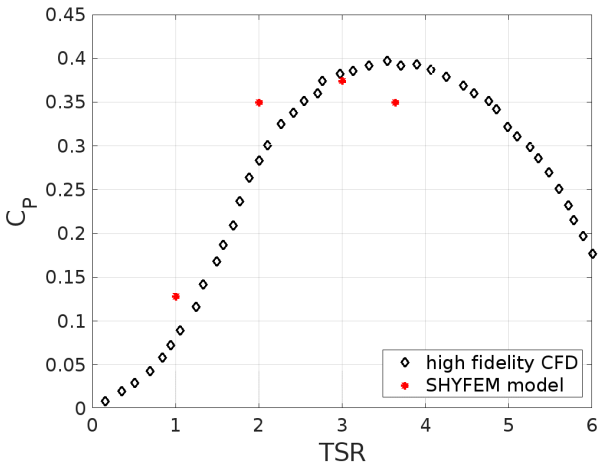

Fig. 2. C_P-TSR curve for a 10 m diameter turbine: comparison between the SHYFEM model (red asterisks) and the high fidelity CFD of [12] (black diamonds.)

between Jensen's model prediction and the SHYFEM simulations results. This is essential for a correct analysis since we use the SHYFEM code to test the power production of the output configurations of the optimization process. This guarantees that differences in power generation of several optimized configurations are not due to a bad representation of the wake in the optimization algorithm.

C. Staggered grid choice

A crucial aspect of the discrete optimization approach is the a-priori choice of the set of fixed positions to choose from. Arguably, a properly chosen set of positions can translate into a better final solution; or, conversely, if the positions are not properly set then optimising over them may lead to less satisfactory results. All previous approaches in the literature used a staggered grid defined by simple rules (cf. $grid_1$ in Fig. 8a), but we posit that choosing a more appropriate staggered grid, taking into account the characteristics of the site where the tidal farm is going to be installed, is possible. In particular, we aim at optimally choosing the distances between the three turbines composing a module, that will be replicated to build the whole grid. That is, we want to chose distances Δx and Δy between turbines T_1, T_2, and T_3 defined as in Fig. 5.
There are some examples of marine sites which exhibit a flow inversion during a flood-ebb cycle which is nearly 180°. Some are found in the Fromveur Strait [14], in Pentland Firth, off the coast near Orkney and near Pembroke [15], off the coast near Amlwch, the Bardsey Sound and the Ramsey Sound [16]. These show a collection of velocity data with a rectilinear or elliptical shape, referring to a polar velocity graph which represents the spread of velocity data as a function of the direction, such as the one shown in Fig. 6. Even if the flood and ebb currents are not perfectly aligned, a prevalent direction (black line in the figure) is clearly present, and we can easily define a tolerance range around this prevailing direction (red lines in the figure).

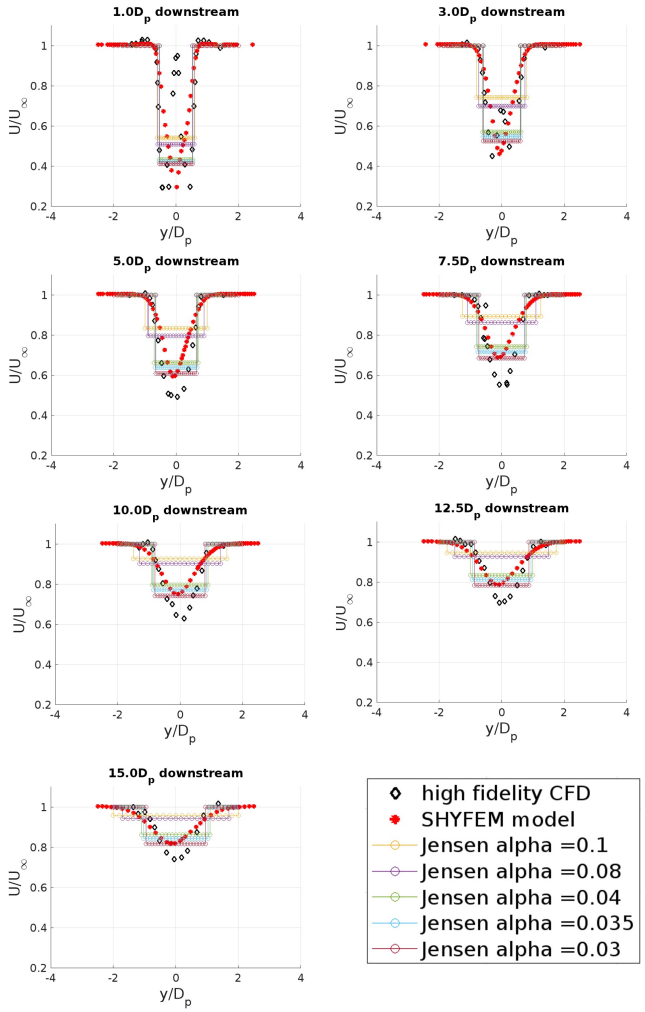

Fig. 3. Wake velocity profiles relative to the horizontal middle plane for a 10 m diameter turbine: comparison between the SHYFEM model (red asterisks) at the optimal TSR i.e. 3, the high fidelity CFD of [11] (black diamonds) at the optimal TSR i.e. 3.64, and the Jensen's wake model with various alpha values.

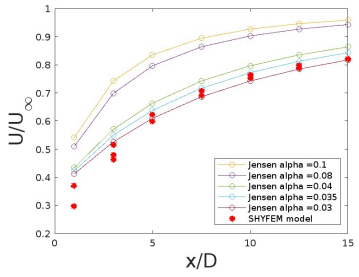

Fig. 4. Comparison between the wake centreline velocity prediction of the Jensen analytical model at various alpha values, and the SHYFEM fluid dynamics simulations (red asterisks).

That is, we consider as exploitable flow velocity all those which fall within the tolerance angle, and consequently we adapt the three turbines module to these directions. In Fig. 5 we denote with θ the tolerance angle around the prevalent direction, i.e., direction 1. Hence, the flow can have a direction ranging between 2 and 3 as in the figure. Once we have placed turbine T_1, we can establish distances Δx and Δy by geometrical arguments. First and foremost we assume that the turbines have a control system able to regulate the yaw angle relative to the incoming flow: hence, the turbines are perpendicular to the flow for each incoming directions.

Let us now consider a flow coming from direction 3: the shaded rectangle in Fig. 5 represents the wake of turbine T_1. Thus, in order for turbine T_2 to remain undisturbed by the wake the following constraint

$$\Delta x \leq \frac{\Delta y}{tan(\theta)} - \frac{2r}{sin(\theta)} \tag{14}$$

must be satisfied. By placing T_3 symmetrically, (14) provides a bound on the maximum distance Δx which avoids wake interference among the three turbines in the module for each incoming flow with directions ranging from 2 to 3. Moreover, a fixed minimum technical distance between the devices equal to 3 turbine diameters D_T is required [7]), which leads to the other constrains

$$\Delta y \geq 1.5 D_T \tag{15}$$

$$\Delta x \geq \begin{cases} 0 & \text{if } \Delta y \geq 3D_T \\ \sqrt{(3D_T)^2 - \Delta y^2} & \text{if } \Delta y < 3D_T \end{cases} \tag{16}$$

In particular, (15) guarantees the minimum technical distance between T_1 and T_3, whereas (16) imposes the minimum technical distance between T_1 and T_2 (and, symmetrically, between T_3 and T_2).

To finally set the values for Δx and Δy we employed an iterative process whereby we vary Δy from the minimum value ($1.5D_T$) to an arbitrarily high value and we compute the constrains for Δx using (14) and (16). Not all the Δy lead to feasible constrains for Δx, and we chose the minimum Δy that does. This choice can be justified in two ways. First, while a large Δy is possible, we know from literature is that beneficial fluid dynamics effects between devices arise if turbines are placed close enough. Moreover, a very high value for Δy would result in a too large grid, running contrary to the objective of keeping the total area of the farm as small as possible.

Once Δy is fixed to the minimum feasible value, Δx can range between what is prescribed in (14) and (16). Our choice falls on the lower bound of Δx, i.e., (16). This can be justified referring to Fig. 7a). The point is that while the three-turbines module has a triangular symmetry in direction 1, an asymmetry arises if we consider direction 3 (or, symmetrically, 2). Indeed, the transversal distances between turbines d_1 and d_2 (with a flow with direction 3) are rather different. Fig. 7b) highlights how the more we place T_2 closer to the lower bound for Δx (the blue point in the figure), the less the difference between d_1 and d_2. In other words, the turbine modules are more symmetric also to direction 3 (and 2, which is specular), ensuring a fairer treatment for all the considered directions. Besides, a smaller Δx also contributes to keeping the farm area small.

III. Case Study

A. Site characterization and set up

As a case study we have considered the site called the Ramsey Sound, proposed in [17]. It is a strait

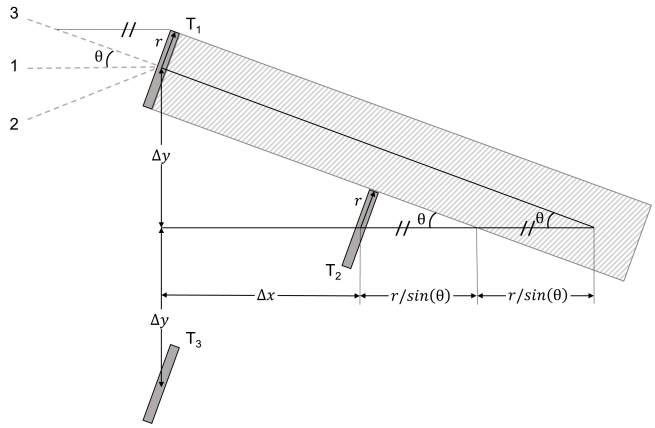

Fig. 5. Schematic representation of a three turbines module. The grey rectangles are turbines T_1, T_2, and T_3.

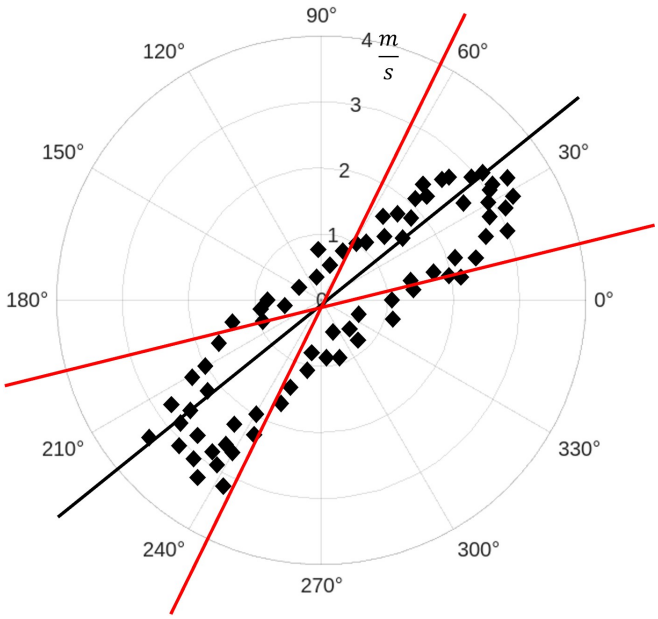

Fig. 6. Qualitative representation of velocity data spread in a site characterized by an elliptical polar graph. We can identify a prevalent direction (black line), and around it consider a tolerance range of directions bounded by the red lines, with suitable velocity for energy exploitation.

located near St. David's headland, Wales, UK, which is 1500-1600m wide and about 3km long, with depth ranging between 20m and 70m. A measurement campaign was conducted [18] which shows that the center of the Sound can be with good approximation considered a bidirectional site, with a north-south dominant direction. Data collected during a flood-ebb cycle show a spread in velocity directions, but the more significant recorded velocities fall into a tolerance range of 20 degrees with respect to the prevalent north-south direction. This means velocities higher than 2m/s during the flood tide, with peaks of 4m/s, with much smaller values during the ebb tide. Since for this specific site the flood phase is the most relevant in terms of energy exploitation, we will focus our analysis only on the flood phase. Therefore, as suggested in [17], an undisturbed flow velocity equal to 3m/s can be considered to characterize the flood tide of the site. Hence, the latter velocity value will be the uniform inlet velocity

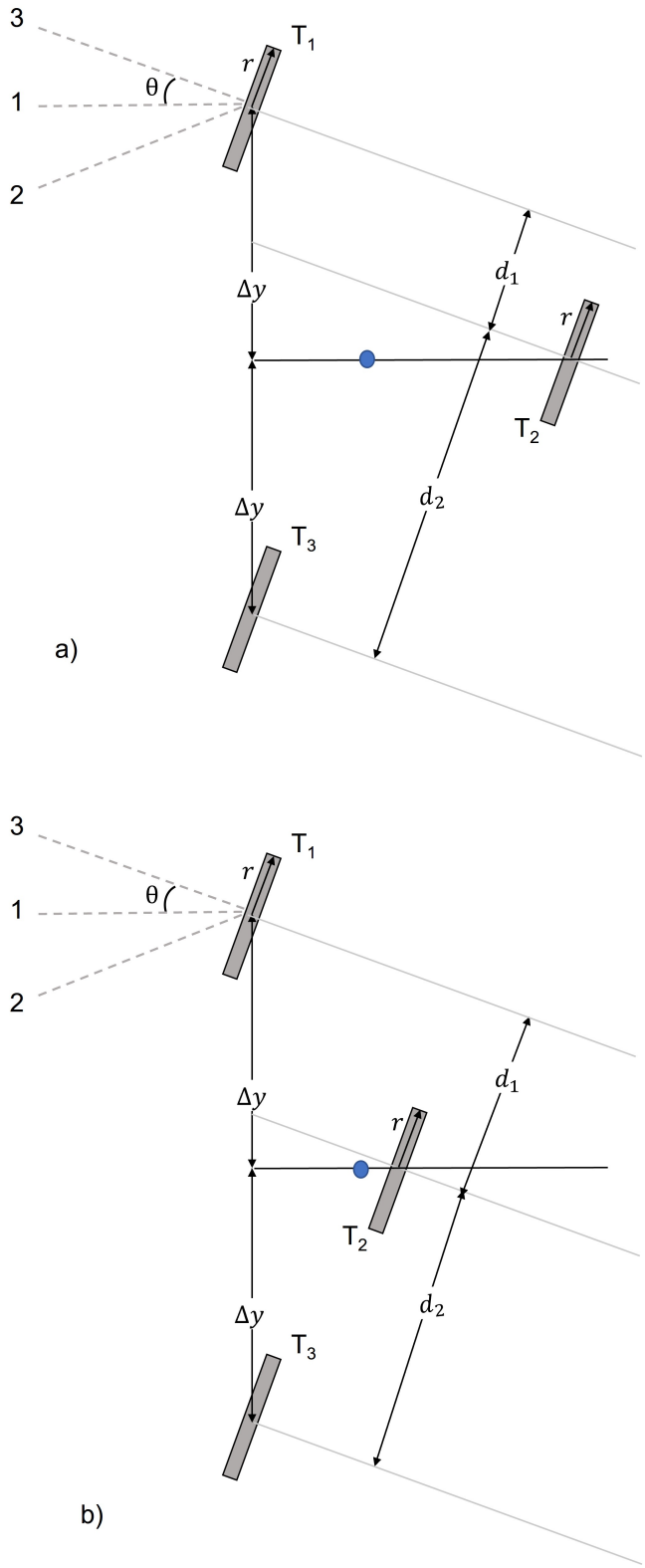

Fig. 7. a) shows the distances between T_1 and T_2 and between T_3 and T_2 perpendicular to the flow direction 3, which are respectively d_1 and d_2. b) shows how the difference in length between d_1 and d_2 can be mitigated by approaching turbine T_2 towards the lower bound for Δx, i.e. the blue point.

for our optimization process, and consequently of our fluid dynamics simulations. The turbine considered has a diameter D_T of 18m, and it is geometrically similar to the one used to test the real size model in section II-B.

We want to analyse the importance of the choice of the

staggered grid given as input to a discrete optimization algorithm. Hence, we assign two different staggered grids as input. The typical choice from the literature, that we will call $grid_1$, has a Δy distance equal to the minimum technical distance (i.e., $1.5D_T$), whereas Δx is equal to $5D_T$ to grant enough wake recovery, as shown in [6], [13]. The site-adapted grid, that we will call $grid_2$, is obtained following the procedure described in the previous section. The θ angle characteristic of the Ramsey Sound is 20 degrees, leading to a minimum feasible distance Δy of $2.5D_T$, and consequently to Δx equal to the lower bound of $1.7D_T$. We have optimized the layout of a small farm made up of 9 devices. Both grids have a 6x6 configuration, hence 36 available locations. The layout outputs from the optimization algorithm are shown in Fig. 8: Fig. 8a) shows the conventional $grid_1$ with $3D_T$-$5D_T$ spacing, and Fig. 8b) the site-adapted $grid_2$ with $5D_T$-$1.7D_T$ spacing. The shaded rectangles indicate the locations occupied by turbines in the optimal design. We then tested the two different farm configurations with fluid dynamics BEM based simulations to attest which one is the best. The calculation domain has a depth of 70 m, and is $58D_T$ wide and $70D_T$ long in case of $grid_1$, whereas it is $70D_T$ wide and $50.2D_T$ long in case of $grid_2$. The grid horizontal resolution goes from 1m in the turbine region to 40m at the domain boundaries. The vertical discretization is equal to 1m over the whole water column, and the turbines are centered in the middle of it. The undisturbed flow velocity is 3m/s as already mentioned.
To test the effectiveness of the site-adapted $grid_2$, and avoid case dependent outcomes, we have use the same two grids (i.e. $grid_1$ and $grid_2$ with 36 available locations and Δx and Δy spacing as described above) to optimize the layout of 18 devices. We will refer as $CaseA$ for the 9 turbines optimization, and as $CaseB$ for the 18 turbines optimization.

B. Results

1) Case A: We have simulated both farm configurations in three different flow directions: direction 1, which represents the prevalent direction, and direction 2 and 3, which are those at the extreme 20 degrees angle from 1. Fig. 9 shows the flow fields for the three flow directions relative to $grid_1$, plotted on the middle horizontal plane. Analogous flow fields for $grid_2$ are shown in Fig. 10. The latter configuration highlights the presence of larger acceleration corridors between devices, and hence a more favourable flow condition. This is confirmed by Fig. 11 where the power outputs of the two farms are plotted: the farm generated from $grid_2$ reaches higher power production for each of the three considered directions. Table I summarizes some data. The total power amount P_{tot}, defined as the sum of power generated at each direction, is about 6% higher in the case of the farm generated from $grid_2$. Moreover, we define as the total horizontal area A_{tot} occupied by the farm as that of the smallest rectangle able to contain the whole farm: the farm obtained with $grid_2$ has a much reduced A_{tot}, leading to a very significant—nearly 10-fold—increase in power density (defined as P_{tot}/A_{tot}).

TABLE I

	$grid_1$	$grid_2$
P_{tot}	33.8 MW	35.8 MW
Power increment	/	+6%
A_{tot}	133650 m^2	15147 m^2
Power density	252.9 W/m^2	2363.5 W/m^2

Comparison between $grid_1$ and $grid_2$ farm in terms of total power production P_{tot}, and Power density for $CaseA$.

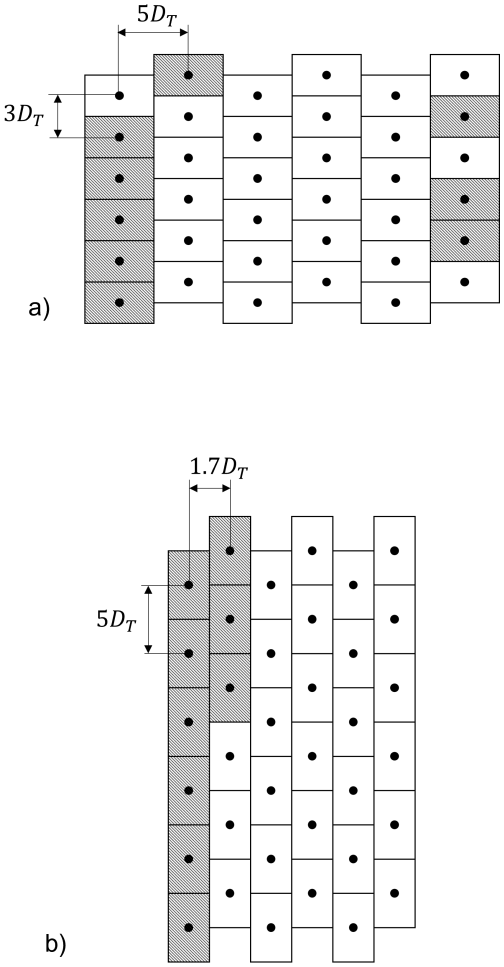

Fig. 8. a) $grid_1$ conventional staggered grid, and b) $grid_2$ site-adapted staggered grid. The shaded rectangles represent locations occupied by the 9 turbines of the cluster we wanted to optimize ($CaseA$).

2) Case B: The left side of Fig. 12 shows the output layouts of 18 devices obtained from the optimization process. The shaded rectangles represents locations occupied by turbines. In analogy to what done for $CaseA$, we performed fluid dynamic simulations to test the three directions of interest. In Fig. 12 we show for brevity, only the flow field relative to direction 1, plotted on the middle horizontal plane. Even in $CaseB$ we record better performance for the farm obtained from $grid2$. The power amount of the whole farm in each direction is shown in Fig. 13. We can notice that $grid_2$-farm achieves higher power generation for each of the directions considered, same trend as $CaseA$. The

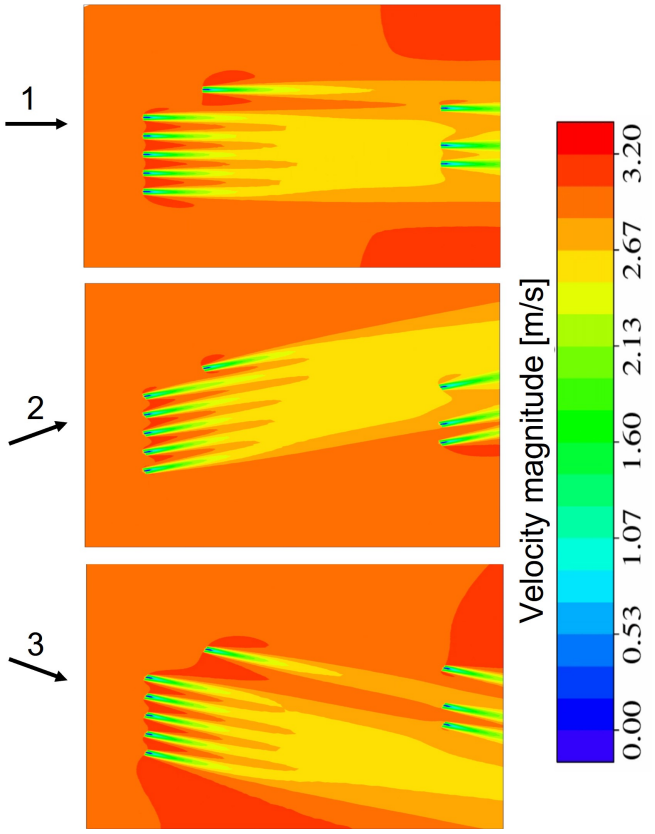

Fig. 9. $grid_1$ flow field of direction 1, 2, and 3 for $CaseA$. The flow fields are plotted on the horizontal middle plane.

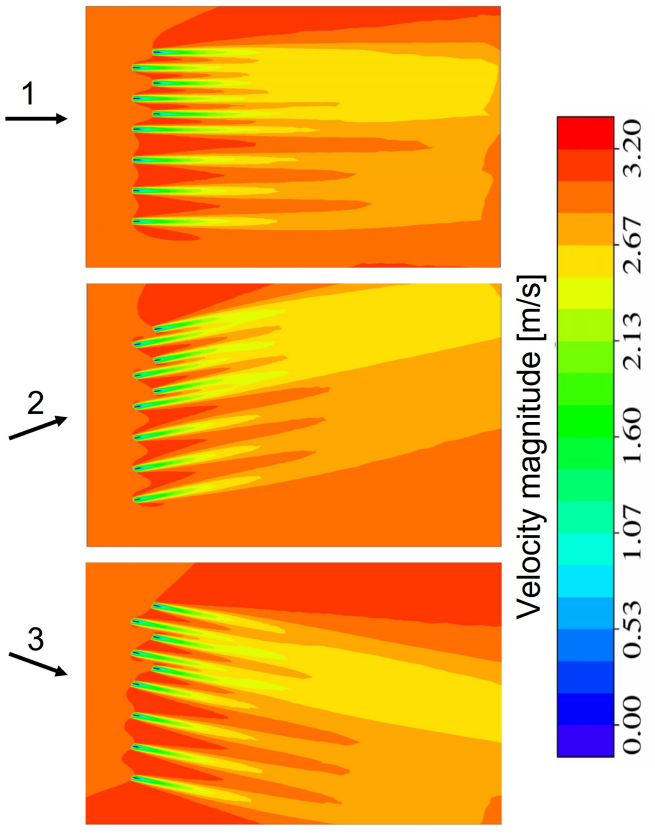

Fig. 10. $grid_2$ flow field of direction 1, 2, and 3 for $CaseA$. The flow fields are plotted on the horizontal middle plane.

total power amount P_{tot}, (sum on the three directions) is about 56MW for $grid_1$ and 66.7MW for $grid_2$, with

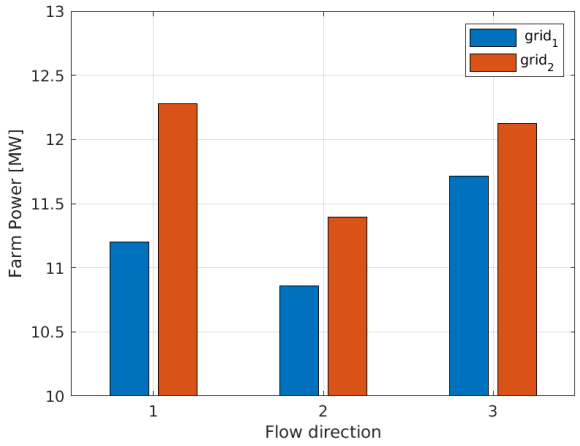

Fig. 11. Power amount of the 9 turbines farm for each flow direction.

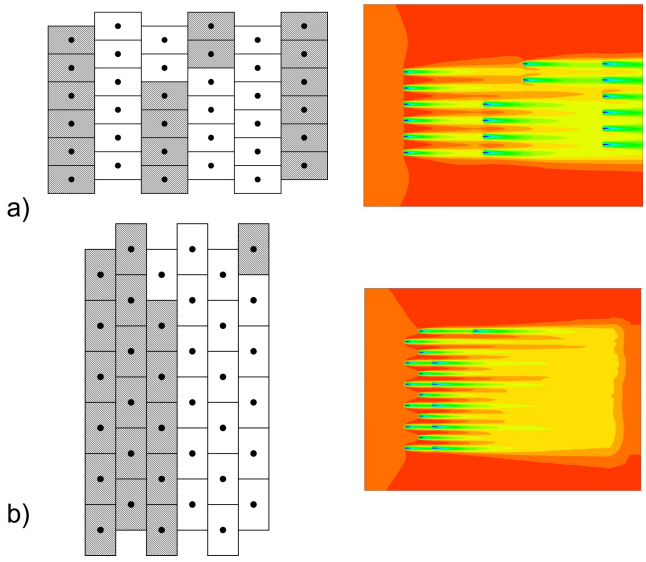

Fig. 12. On the left the optimized configuration for 18 turbines, on the right the flow field relative to direction 1 respectively for a) $grid_1$, and b) $grid_2$. The colour-map is the same as in Fig.9 and 10

an increase of about 19% in case of $grid_2$. Again the power density is enhanced, since the total area A_{tot} occupied by the farm is in both cases equal to the total area of the grid. Indeed, $grid_2$ has a lower superficial extension (36 rectangles $1.7D_T \times 5D_T$ instead of 36 rectangles $5D_T \times 3D_T$), therefore the power density is increased almost 2-fold. Hence, even studying a farm made up of a larger number of turbines (half of the available locations), the growth in total power and power density is still achieved.

C. Sensitivity analysis

Since it is practically unfeasible to simulate an infinitely large domain for a farm, we wanted to guarantee that the extension of the domains used are large enough to prevent relevant blockage effects. The domains used to simulate $grid_1$ and $grid_2$ farms where obtained by maintaining $20D_T$ of distance from the extreme points of the staggered grid. Considering Fig. 8, we maintained $20D_T$ in direction North, South, East and West from the boundary location plotted in the

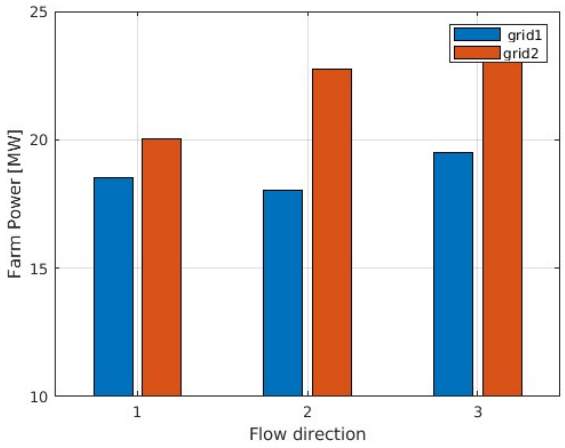

Fig. 13. Power amount of the 18 turbines farm for each flow direction.

TABLE II
SENSITIVITY ANALYSIS

domain	Power	Δ %
+10%	12.16 MW	-0.78%
+20%	12.2 MW	-0.3%

Power outputs of the 9 turbines farm from the sensitivity analysis performed by enhancing the domain width. The $\Delta\%$ column indicates the percentage difference in power outputs with respect to the original domain.

grid.

We made a sensitivity analysis to the domain extension by performing further simulations of the farm obtained with $grid_2$, considering only the flow direction 1. In this case, we enlarged the domain (in the direction perpendicular to the flow) of +10% and +20%, passing from a $70D_T$ wide domain, to a $77D_T$ and a $84D_T$ wide domain respectively.

Table II reports the power outputs of the simulations, with Δ denoting the percentage difference in power output with respect to the original domain. Differences are negligible, hence we can conclude that the original chosen domains were large enough to avoid significant blockage effects.

IV. CONCLUSION

In this paper, we analysed the layout optimization of tidal turbines farms. Since, most of the works in this field employs a discrete optimization approaches to maintain low computational costs, we studied the importance of the discretization choice. Indeed, we have shown how a discretization only made by using literature assumptions (which was the $grid_1$ case in this paper) can be significantly improved. The tailor made discretization ($grid_2$) was built taking into consideration the flow characteristics of the site chosen for the farm installation. The module of three turbines, replicated to build $grid_2$, was obtained from simple geometrical evaluations. Nonetheless, for a small cluster of 9 turbines, we have obtained an increase in power production of 6% with respect to the standard grid. Moreover, the power density (i.e., the ratio between the power production and the sea area occupied by the farm) has increased by nearly 10 times. This is significant result: indeed, a reduction in the sea area extension reserved for energy purposes have positive repercussions from an environmental point of view, and also provides space for the other stakeholders activities.

To avoid case-dependent conclusions, we also tested a farm of 18 devices: again, the power production and power density achieved, are greater for the $grid_2$ farm. The power production is about 19% higher than the $grid_1$ farm.

Further development of this research could be obtained by making more complex fluid dynamics evaluations on the module of the three turbines. Indeed, it could be possible to perform a set of fluid dynamic simulations to detect the best module configuration: in this case, we will also be able to better exploit favourable flow conditions in terms of a beneficial mutual influence among the turbines in the module.

REFERENCES

[1] A. S. Sleiti, "Tidal power technology review with potential applications in gulf stream," *Renewable and Sustainable Energy Reviews*, vol. 69, pp. 435–441, 2017.
[2] N. O. Jensen, *A Note on Wind Generator Interaction*, D. Riso National Laboratory, DK-4000 Roskilde, Ed., 1983.
[3] S. D. O. Turner, D. A. Romero, P. Y. Zhang, C. H. Amon, and T. C. Y. Chan, "A new mathematical programming approach to optimize wind farm layouts," *Renewable Energy*, vol. 63, pp. 674–680, 2014.
[4] R. Archer, G. Nates, S. Donovan, and H. Waterer, "Wind Turbine Interference in a Wind Farm Layout Optimization Mixed Integer Linear Programming Mode," *Wind Engineering*, vol. 35, no. 2, pp. 165–178, 2011.
[5] M. M. Aguayo, P. E. Fierro, R. A. De la Fuente, I. A. Sepúlveda, and D. M. Figueroa, "A mixed-integer programming methodology to design tidal current farms integrating both cost and benefits: A case study in the Chacao Channel, Chile," *Applied Energy*, vol. 294, 2021.
[6] R. Vennel, S. W. Funke, S. Draper, C. Stevens, and T. Divett, "Designing large arrays of tidal turbines: A synthesis and review," *Renewable and Sustainable Energy Reviews*, vol. 41, pp. 454–472, 2015.
[7] S. Nasha and A. Phoenixa, "A review of the current understanding of the hydro-environmental impacts of energy removal by tidal turbines," *Renewable and Sustainable Energy Reviews*, vol. 80, p. 648–662, 2017.
[8] C. H. Jo, J. H. Lee, Y. H. Rho, and K. H. Lee, "Performance analysis of a HAT tidal current turbine and wake flow characteristics," *Renewable Energy*, vol. 65, pp. 175–182, 2014.
[9] [Online]. Available: https://github.com/SHYFEM-model/shyfem
[10] M. Pucci, C. Di Garbo, D. Bellafiore, S. Zanforlin, and G. Umgiesser, "A BEM-Based Model of a Horizontal Axis Tidal Turbine in the 3D Shallow Water Code SHYFEM," *J. Mar. Sci. Eng.*, vol. 10(12), 2022.
[11] S. Salunkhe, "Model- and full-scale predictions of hydrokinetic turbulent wake, including model-scale validation," 2016.
[12] A. Mason-Jones, D. M. O'Doherty, C. E. Morris, T. O'Doherty, C. B. Byrne, P. W. Prickett, R. Grosvenor, I. Owen, S. Tedds, and R. Poole, "Non-dimensional scaling of tidal stream turbines," *Energy*, vol. 44, pp. 820—-829, 2012.
[13] O. A. Lo Brutto, J. Thiébot, S. S. Guillou, and H. Gualous, "A semi-analytic method to optimize tidal farm layouts – Application to the Alderney Race (Raz Blanchard), France," *Applied Energy*, vol. 183, pp. 1168–1180, 2016.
[14] T. El Tawin, N. Guillou, J. Charpentier, and M. Benbouzid, "On Tidal Current Velocity Vector Time Series Prediction: A Comparative Study for a French High Tidal Energy Potential Site," *Journal of Marine Science and Engineering*, vol. 7, no. 46, 2019.

[15] M. Lewis, R. Hashemi, S. Neill, and P. Robins, "The direct effect of waves on the tidal stream energy resource." International Conference on Renewable Energies Offshore, Portugal, Lisbon, 2015, pp. 169–176.
[16] M. Piano, S. P. Neill, M. J. Lewis, P. E. Robins, M. R. Hashemi, A. G. Davies, S. L. Ward, and M. J. Roberts, "Tidal stream resource assessment uncertainty due to flow asymmetry and turbine yaw misalignment," *Renewable Energy*, vol. 114, pp. 1363–1375, 2017.
[17] C. H. Frost, P. S. Evans, M. J. Harrold, A. Mason-Jones, T. O'Doherty, and D. M. O'Doherty, "The impact of axial flow misalignment on a tidal turbine," *Renewable Energy*, vol. 113, pp. 1333–1344, 2017.
[18] P. Evans, A. Mason-Jones, C. Wilson, C. Wooldridge, T. O'Doherty, and D. O'Doherty, "Constraints on extractable power from energetic tidal straits," *Renewable Energy*, vol. 81, pp. 707–722, 2015.